Chinese Chemical Letters 33 (2022) 851–854

Contents lists available at ScienceDirect

Chinese Chemical Letters

journal homepage: www.elsevier.com/locate/cclet

Cucurbit[8]uril-mediated phosphorescent supramolecular foldamer for antibiotics sensing in water and cells

De-Ao Xu, Qing-Yang Zhou, Xianyin Dai, Xin-Kun Ma, Ying-Ming Zhang*, Xiufang Xu, Yu Liu*

College of Chemistry, State Key Laboratory of Elemento-Organic Chemistry, Nankai University, Tianjin 300071, China

ARTICLE INFO

Article history:
Received 20 June 2021
Revised 18 July 2021
Accepted 2 August 2021
Available online 8 August 2021

Keywords:
Supramolecular assembly
Cucurbiturils
Supramolecular foldamer
Phosphorescence sensing
Antibiotics detection

ABSTRACT

A phosphorescent supramolecular foldamer is conveniently constructed by the 1:1 host–guest complexation with cucurbit[8]uril and 1,2-diaminocyclohexane-bridged 4-(4-bromophenyl)-pyridinium salt. The tightly compact host–guest complexation in molecular foldamer can greatly suppress the fluorescence emissive channel and promote the intersystem crossing from singlet to triplet states, thus leading to the green phosphorescence at ambient temperature in aqueous solution. More intriguingly, the phosphorescence emission shows very rapid and sensitive responsiveness to different antibiotics in both inanimate milieu and living cells. Remarkably, the limit of detection of such binary inclusion complex toward sulfamethazine can reach as low as 1.86×10^{-7} mol/L. Thus, it is envisaged that this supramolecular nanoplatform featuring unique complexation-enhanced phosphorescence emission may hold great promise in sensing and detecting many other biological targets under physiological environment.

Light-emitting nanoconstructs based on cavity-bearing macrocyclic compounds have drawn extensive attention due to their unique photophysical performance and promising applications in material science [1–3] and biological technology [4,5]. The studies on photoactive supramolecular assemblies have been recently extended from fluorescence- to phosphorescence-based purely organic nanosystems with persistent room-temperature luminescence [6,7], because the latter has more immense advantages, such as longer lifetime [8], larger Stokes shift [9], and their reliability and practicability under biological environments [10]. In this context, host–guest complexation with cucurbiturils (CBs), a family of carbonyl-rich macrocycles with rigidified molecular skeletons [11,12], can greatly reduce the nonradiative decay and promote the intersystem crossing (ISC) from singlet to triplet states through multiple cooperative noncovalent interactions [13,14], thus facilitating the enhancement of phosphorescence emission in solution [15] and solid state (Scheme 1a) [16]. Consequently, diverse CB-enhanced phosphorescent nanostructures with peculiar topological features and physicochemical functionalities have been investigated over the past few years, which have greatly broadened the research scope for photoactive supramolecular nanoassemblies. Nevertheless, besides the optimization of photophysical performance, the utilization of macrocycle-binding-induced room-temperature phosphorescence (RTP) for effective sensing and detection under aqueous/physiological environments is still challenging.

Antibiotics are a type of medications directed against bacterial infection. Although they have anti-pathogen and other vital bioactivities in the life process, the extensive misuse and abuse of antibiotics can eventually lead to severe drug resistance and environmental pollution. Therefore, the development of advanced and efficient sensing and detection methods toward antibiotics is highly imperative. However, most popular antibiotic-sensing methods and technologies are derived from liquid chromatography, mass spectrometry, and capillary electrophoresis [17], which are time-consuming and require installation and operation of costly instruments. In this work, a supramolecular foldamer was constructed by the host–guest complexation between 1,2-diaminocyclohexane-bridged 4-(4-bromophenyl)-pyridinium salt (**G**) and cucurbit[8]uril (CB[8]), which can produce strong complexation-induced RTP in aqueous media. The linear **G** molecule can be driven by the CB[8]-involved complexation to adopt a foldamer-like secondary structure [18]. Significantly, the phosphorescence emission has ultrahigh sensitivity toward selected antibiotics (Scheme 1b). Moreover, phosphorescence imaging results showed that the biocompatible **G**⊂CB[8] supramolecular foldamer can be further applied in the detection of excessive antibiotics in living cells. Since there is a relative paucity of studies on the supramolecularly RTP-based sensing

* Corresponding authors.
E-mail addresses: ymzhang@nankai.edu.cn (Y.-M. Zhang), yuliu@nankai.edu.cn (Y. Liu).

https://doi.org/10.1016/j.cclet.2021.08.001
1001-8417/

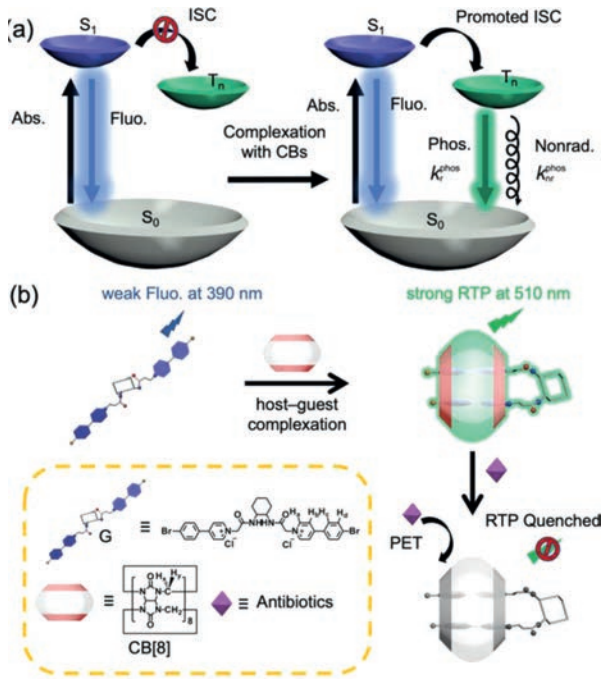

Scheme 1. (a) Illustration of the Jablonski diagram for radiative and non-radiative processes *via* CB-based supramolecular regulation strategy. (b) Schematic representation and proton designation of 1:1 host–guest complex between **G** and CB[8] and its phosphorescent sensing toward antibiotics.

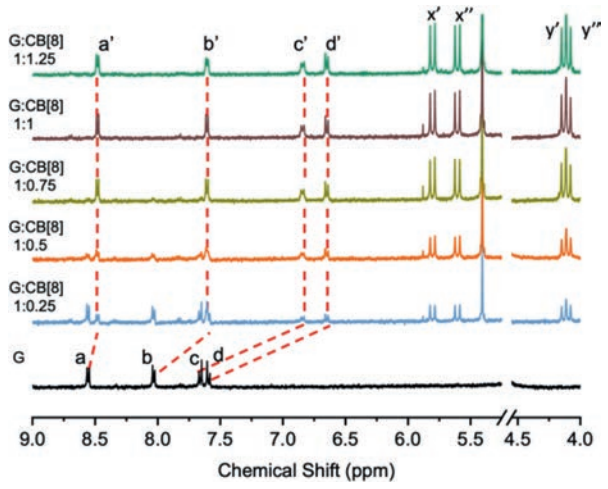

Fig. 1. Partial ^{1}H NMR spectra of **G** upon addition of CB[8] in D_2O at 25 °C ([**G**] = 0.2 mmol/L).

platforms toward antibiotics, our work may open up a new direction for the application of purely organic RTP in the bio-related fields.

The homoditopic pyridinium guest **G** was synthesized by the reaction of 4-(4-bromophenyl)pyridine and chlorinated 1,2-diaminocyclohexane (Figs. S1–S3 in Supporting information). The proton signals of aromatic moieties (H_{a-d}) underwent a dramatic complex-induced upfield shift upon addition of CB[8] with slow dynamics, indicating that the 4-(4-bromophenyl)-pyridinium moiety was encapsulated in the cavity of CB[8]. The chemical shift changes of proton signals of **G** reached the equilibrium state with 1 equiv. of CB[8] (Fig. 1). After validating the 1:1 binding stoichiometry by Job plot, the binding constant (K_S) was measured as 2.59×10^6 L/mol using the nonlinear least-squares curve-fitting method (Figs. S4 and S5 in Supporting information).

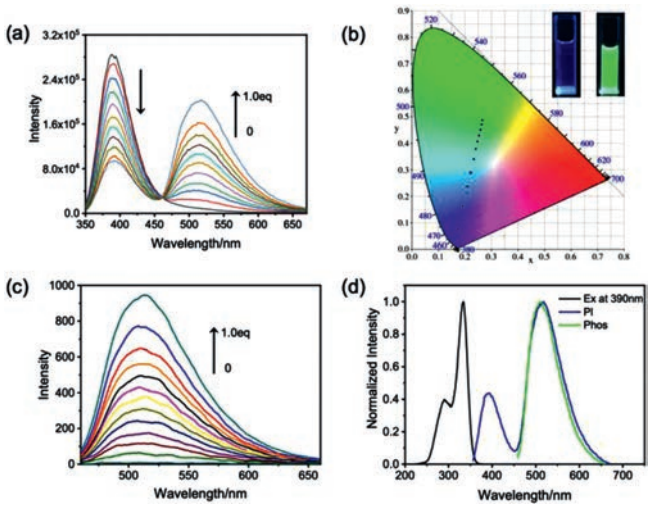

Fig. 2. (a) Photoluminescence spectra of **G** (50 μmol/L) with 0–1.0 equiv. of CB[8] in water (λ_{ex} = 340 nm). (b) The CIE 1931 chromaticity diagram of **G** with different molar ratios of CB[8] in water in accordance with (a). Inset: photographs of **G** before (left) and after (right) addition of 1.0 equiv. of CB[8] in water. (c) Phosphorescence emission spectra of **G** (50 μmol/L) in the presence of 0–1.0 equiv. of CB[8] in water (delayed by 0.1 ms, λ_{ex} = 340 nm). (d) Normalized excitation, photoluminescence and phosphorescence (delayed by 0.1 ms) spectra of **G**⊂CB[8] complex in water.

Diffusion-ordered NMR spectra (DOSY) showed that the diffusion coefficients of **G** and **G**⊂CB[8] at 1.0 mmol/L were determined as 3.62×10^{-10} and 2.83×10^{-10} m^2/s, respectively (Fig. S7 in Supporting information). These diffusion coefficients indicate the quite similar molecular sizes between **G** and **G**⊂CB[8] complex [19]. In addition, no change in chemical shifts of the guest molecule **G** was observed in the ^{1}H NMR spectra of **G**⊂CB[8] complex at different concentrations (Fig. S8 in Supporting information). These results demonstrated that the structure of **G**⊂CB[8] complex was fairly stable in the diluted solution and no large-sized polymeric species was formed even at relatively higher concentration. Moreover, after scrutinizing the peak pattern of **G**⊂CB[8] complex, the resonance peaks of interior protons (H_{x-y}) in CB[8] host were split into two identical sets. This phenomenon indicates that two carbonyl-laced portals of CB[8] were located in an asymmetric environment dominated by different positive-charge distribution.

The formation of a 1:1 binary species was further evaluated by mass spectrometry. The intense *m*/*z* peak at 996.2459 could be assigned to $[\mathbf{G} + CB[8] - 2Cl]^{2+}$ and the interval of two adjacent peaks was observed as 0.5 in the electrospray-ionization mass spectrometry (Fig. S9 in Supporting information). In addition, no discrete *n*:*n* complex with CBs (n > 1) was found in the ion-mobility mass spectrum (Fig. S10 in Supporting information) [20,21]. Taken together, we can reasonably propose a foldamer-based 1:1 binding mode for the binary **G**⊂CB[8] complex, in which two pyridine moieties of the guest molecule make close contact with each other at one carbonyl-laced portal of CB[8] and may adopt partially overlapping conformation in the CB[8] cavity, thus leaving the cyclohexyl center outside the cavity [22]. This 1:1 binding mode is largely contributed to the existence of flexible cyclohexyl moiety, which is distinctive from the 2:2 host–guest system possessing a rigidified linker group [15].

Subsequently, the photophysical behaviors of 1:1 foldamer-like **G**⊂CB[8] complex was investigated. As shown in Fig. 2a, the emission peak of **G** initially appeared at 390 nm, accompanied by the steady enhancement at 510 nm upon addition of CB[8]. No similar phenomenon was observed for **G** with the homologue of cucurbit[7]uril (CB[7], Fig. S11 in Supporting information). The CIE 1931 chromaticity diagram further showed the emission color changes,

exhibiting weak blue and strong green photoluminescence before and after addition of CB[8], respectively (Fig. 2b). Time-resolved photoluminescence spectroscopy (delayed by 0.1 ms) further corroborates the strong phosphorescence emission by **G**⊂CB[8] complex at 510 nm (Figs. 2c and d). To confirm whether the new peak at 510 nm came from phosphorescence emission, the steady-state spectrum was recorded after argon was bubbled into the solution. As expected, when bubbling with argon, the **G**⊂CB[8] solution showed an enhanced emission peak at 510 nm, whereas no appreciable change was observed for the oxygen-insensitive fluorescence emission at 390 nm, indicating that the photoluminescence in the long-wavelength region is originated from triplet state (Fig. S12 in Supporting information). Furthermore, as shown in Figs. S13a and b (Supporting information), as the temperature decreased, the phosphorescence intensity and lifetime gradually increased, from which the possibility of thermally activated delayed fluorescence should be excluded [23,24]. Therefore, we can clearly refer that the favorable RTP in aqueous solution is achieved in the supramolecular foldamer.

To better understand the phosphorescence generation mechanism of **G**⊂CB[8] foldamer, quantitative calculations were performed using the density functional theory (DFT) and time-dependent DFT (TD-DFT). As shown in Fig. S13c (Supporting information), the optimized structure showed that the phenylpyridinium moiety of guest molecule was wrapped in the CB[8] cavity, which could prohibit the non-radiative transition and deter the guest molecule from self-quenching in aqueous solution. Meanwhile, the guest molecules adopted a head-to-head form with favorable π-stacking interaction in the cavity of CB[8]. All these favorable molecular conformations are believed to enhance the ISC pathway. Indeed, theoretical calculations showed that there were many feasible ISC channels between the involved singlet state and triplet states ($S_1 \rightarrow T_n$) and the energy gaps between S_1 and T_n (ΔE_{ST}, n = 3–6) were lower than 0.3 eV (Fig. S13d in Supporting information). Therefore, the combination of low ΔE_{ST} and relatively larger spin-orbit coupling (SOC) coefficients could be jointly contributed to the favorable RTP emission in aqueous solution [25].

Time-resolved fluorescence and phosphorescence decay curves of **G**⊂CB[8] complex were then measured (Figs. S14 and S15 in Supporting information). The lifetime (τ) of the emission at 390 nm was determined to be 176.9 ps, corresponding to the short-lived fluorescence-emission species. In contrast, the emission at 510 nm gave a much longer lifetime on the order of microseconds under ambient condition (τ = 0.77 ms) and the τ value further increased to 3.18 ms under argon atmosphere. Meanwhile, quantum yield (Φ) tests showed the **G**⊂CB[8] complex had strong phosphorescent emission of 8.4% quantum yield. Also, lacking oxygen as quencher, the quantum yield of **G**⊂CB[8] complex could be enhanced to 15.1% under argon atmosphere (Figs. S16 and S17 in Supporting information). The ISC rate constant (k_{isc}), and the radiative and nonradiative decay rate constants (k_r^{phos} and k_{nr}^{phos}) phosphorescence were accordingly calculated as 4.76×10^8, 1.09×10^2, and 1.19×10^3 s^{-1}, respectively (Table S1 in Supporting information) [26].

We next tested the photoluminescence spectral changes in the presence of some antibiotics. Sulfamethazine (SMZ), a sulfanilamide-derived anti-infective agent and an environmental contaminant, was selected as the drug analyte (Fig. 3a). As judged from Fig. 3b, the photoluminescence emission of **G**⊂CB[8] complex was seriously quenched upon addition of SMZ. The phosphorescence emission at 510 nm could be sharply declined upon the addition of 0.5 equiv. of SMZ, while no obvious change was observed for the fluorescence emission at 390 nm. The luminescent color of the SMZ@(**G**⊂CB[8]) solution simultaneously turned from light green to blue. In addition, the phosphorescent sensing behaviors of

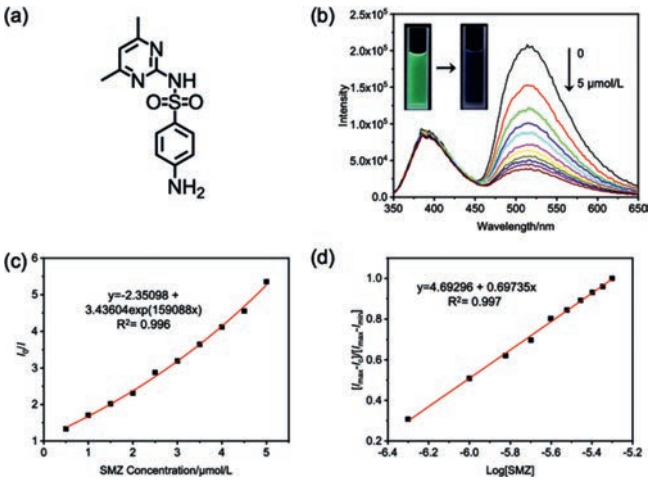

Fig. 3. (a) Molecular structure of SMZ. (b) Photoluminescence spectra of **G**⊂CB[8] complex ([**G**] = [CB[8]] = 10 μmol/L) with addition of SMZ (0–5 μmol/L) in aqueous solution (λ_{ex} = 340 nm, Inset: photographs of **G**⊂CB[8] complex before and after addition of SMZ). (c) Stern-Volmer plot of **G**⊂CB[8] complex upon addition of SMZ in aqueous solution. (d) $(I_{max} - I)/(I_{max} - I_{min})$ *vs.* Log[SMZ] plots in aqueous solution.

G⊂CB[8] complex toward SMZ was also investigated by the Stern-Volmer relationship. The quenching constant ($K_{S\text{-}V}$) and the limit of detection (LOD value) were calculated as 1.59×10^5 L/mol and 1.86×10^{-7} mol/L, respectively (Figs. 3c and d).

The investigation on photoluminescent sensing behaviors of **G**⊂CB[8] complex has been extended to other antibiotics, including nitrofurazone (NFZ), nitrofurantoin (NFT), metronidazole (MNZ), imipenem (IPN) and thiamphenicol (TPN, Fig. S18 in Supporting information). As shown in Fig. S19 (Supporting information), the photoluminescence titration spectra and quenching efficiency of **G**⊂CB[8] complex toward different analytes were obtained, revealing that SMZ, NFT and NFZ gave much higher quenching efficiency. The absorption of the **G**⊂CB[8] foldamer had small spectral overlap with most of used antibiotics at 340 nm (Fig. S20 in Supporting information). However, given that the fluorescence intensity of **G**⊂CB[8] complex at 390 nm was almost unchanged in the antibiotics-sensing process, the attenuation of excitation energy arising from the overlapped absorption bands as a predominant role can be ruled out. Also, the UV-vis absorption of selected antibiotics was not significantly changed before and after addition of CB[8], suggesting that the guest molecule **G** could not be expelled from the CB[8] cavity by the competitive binding of antibiotics (Fig. S21 in Supporting information). Therefore, the mechanism behind the antibiotics-induced quenching of **G**⊂CB[8] phosphorescence probably results from the photoinduced electron transfer (PET) from **G**⊂CB[8] in an excited state to antibiotics, which is generally accepted as one of main sensing pathways in the luminescence detection for antibiotics [27,28].

In order to verify this PET mechanism, the phosphorescence lifetimes (τ) were measured after adding different concentrations of SMZ. As shown in Fig. S22 (Supporting information), the fitting of $1/\tau$ *vs.* [SMZ] gave a good linear plot and the slope of the Stern-Volmer plot (k_q) was obtained as 1.08×10^9 L mol^{-1} s^{-1}, corresponding to a typical electron transfer reaction controlled by diffusion [29]. Then, quantum chemical calculations were performed to confirm the electron-transfer pathway. As shown in Figs. S23–S25 (Supporting information), the highest occupied molecular orbital (HOMO) of the antibiotics lay at a higher energy level than the lowest unoccupied molecular orbital (LUMO) of **G**⊂CB[8] complex. Thus, upon excitation at the T_1 state, it is favorable to realize electron transfer from antibiotics to the **G**⊂CB[8] complex and cause the phosphorescence quenching [30]. Besides, it is found that

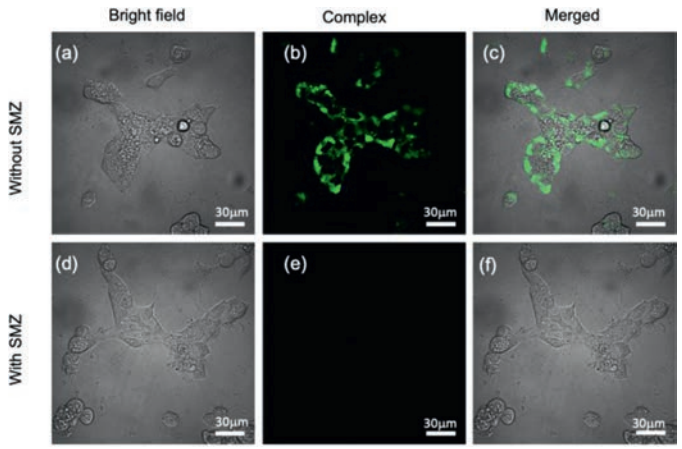

Fig. 4. Confocal laser scanning microscopic images of 293T cells incubated with (a–c) **G**⊂CB[8] complex ([**G**] = [CB[8]] = 10 μmol/L) and (d–f) SMZ and **G**⊂CB[8] complex ([SMZ] = 10 μmol/L).

the energy gaps between the calculated S_0 state and the antibiotics were too large to allow the electron transfer or concomitant fluorescence quenching. The energy gaps between the HOMO of different antibiotics and the β-LOMO of **G**⊂CB[8] complex were also calculated (Fig. S26 and Table S2 in Supporting information). Taking NFZ and TPN as examples, the former with low value of energy gap could result in strong quenching effect toward the phosphorescence of **G**⊂CB[8] complex, whereas the latter with high value (> 0.6 eV) had no obvious quenching ability. These theoretical calculation results are basically consistent with the experimental observation.

Finally, the applicability of phosphorescent antibiotics sensing was examined in the living cells. The safety of **G**⊂CB[8] foldamer was evaluated by measuring the cellular viability of human embryonic kidney cell line (293T). After incubation at different concentrations ranging from 10 μmol/L to 150 μmol/L for 12 h, over 90% cell viability was maintained, due to the nontoxicity and good biocompatibility of **G**⊂CB[8] complex (Fig. S28 in Supporting information). Meanwhile, strong green phosphorescence was observed in the 293T cells under laser irradiation by confocal laser scanning microscopy, indicating that the obtained **G**⊂CB[8] complex could be easily internalized in cells and showed unconventional phosphorescent bioimaging ability without undesired interference (Figs. 4a–c). In keen contrast, when the cell line was co-incubated with SMZ and **G**⊂CB[8] complex, the phosphorescence emission was effectively quenched under the same experimental condition (Figs. 4d–f). These results demonstrate that the phosphorescent sensing of **G**⊂CB[8] complex toward antibiotics could be well applied under cellular environment. Since the phosphorescence-based detection methods have lower background interference and longer lifetime, the complexation-induced phosphorescence may have more potential applications in many other biological fields.

In conclusion, the present study demonstrates that benefitting from the tight encapsulation with CB[8], the homoditopic pyridinium guest **G** can adopt an intramolecular folding mode with 1:1 host–guest complexation, which can produce strong RTP emission in aqueous solution (τ = 0.77 ms, ϕ = 8.4%). Significantly, the obtained phosphorescent **G**⊂CB[8] foldamer could selectively detect SMZ, NFZ and NFT *via* PET process in both inanimate milieu and living cells. Thus, we can envision that the unique phosphorescent antibiotics-sensing properties can not only promote our molecular-level understanding of the nature of purely organic RTP phenomena but also expedite the development of supramolecularly self-assembled RTP materials for environmental monitoring and disease treatments.

Declaration of competing interest

The authors report no declarations of interest.

Acknowledgments

This work was financially supported by the National Natural Science Foundation of China (Nos. 21871154, 21772099, 21861132001, and 21873051) and the Fundamental Research Funds for the Central Universities, Nankai University.

Supplementary materials

Supplementary material associated with this article can be found, in the online version, at doi:10.1016/j.cclet.2021.08.001.

References

[1] Z. Liu, X. Dai, Y. Sun, Y. Liu, Aggregate 1 (2020) 31–44.
[2] M. Rao, W. Wu, C. Yang, Green Synth. Catal. 2 (2021) 131–144.
[3] H. Lai, T. Zhao, Y. Deng, et al., Chin. Chem. Lett. 30 (2019) 1979–1983.
[4] Y.H. Liu, H.J. Yu, Y.M. Zhang, Y. Liu, Angew. Chem. Int. Ed. 60 (2021) 3870–3880.
[5] P. Li, Y. Chen, Y. Liu, Chin. Chem. Lett. 30 (2019) 1190–1197.
[6] T. Zhang, X. Ma, H. Wu, et al., Angew. Chem. Int. Ed. 59 (2020) 11206–11216.
[7] X. Ma, J. Wang, H. Tian, Acc. Chem. Res. 52 (2019) 738–748.
[8] W. Zhao, T.S. Cheung, N. Jiang, et al., Nat. Commun. 10 (2019) 1595.
[9] X.F. Wang, W.J. Guo, H. Xiao, et al., Adv. Funct. Mater. 30 (2020) 1907282.
[10] X.F. Wang, H. Xiao, P.Z. Chen, et al., J. Am. Chem. Soc. 141 (2019) 5045–5050.e.
[11] Q. Cheng, S. Li, Y. Ma, H. Yin, R. Wang, Chin. Chem. Lett. 31 (2020) 1235–1238.
[12] C. Gao, Q. Huang, Q. Lan, et al., Nat. Commun. 9 (2018) 2967.
[13] G. Feng, G.Q. Zhang, D. Ding, Chem. Soc. Rev. 49 (2020) 8179–8234.
[14] Y. Liu, G. Zhan, Z.W. Liu, Z.Q. Bian, C.H. Huang, Chin. Chem. Lett. 27 (2016) 1231–1240.
[15] J. Wang, Z. Huang, X. Ma, H. Tian, Angew. Chem. Int. Ed. 59 (2020) 9928–9933.
[16] Z.Y. Zhang, Y. Chen, Y. Liu, Angew. Chem. Int. Ed. 58 (2019) 6028–6032.
[17] K. Granelli, C. Elgerud, A. Lundstrom, A. Ohlsson, P. Sjoberg, Anal. Chim. Acta 637 (2009) 87–91.
[18] Z.Q. Wu, X.B. Shao, C. Li, et al., J. Am. Chem. Soc. 127 (2005) 17460–17468.
[19] J. del Barrio, P.N. Horton, D. Lairez, et al., J. Am. Chem. Soc. 135 (2013) 11760–11763.
[20] G. Wu, M. Olesinska, Y. Wu, D. Matak-Vinkovic, O.A. Scherman, J. Am. Chem. Soc. 139 (2017) 3202–3208.
[21] S. Combes, K.T. Tran, M.M. Ayhan, et al., J. Am. Chem. Soc. 141 (2019) 5897–5907.
[22] X. Yang, R. Wang, A. Kermagoret, D. Bardelang, Angew. Chem. Int. Ed. 59 (2020) 21280–21292.
[23] X.K. Ma, W. Zhang, Z. Liu, et al., Adv. Mater. 33 (2021) 2007476.
[24] J.X. Wang, Y.G. Fang, C.X. Li, et al., Angew. Chem. Int. Ed. 59 (2020) 10032–10036.
[25] W. Zhao, Z. He, B.Z. Tang, Nat. Rev. Mater. 5 (2020) 869–885.
[26] P.C. Chow, S. Albert-Seifried, S. Gelinas, R.H. Friend, Adv. Mater. 26 (2014) 4851–4854.
[27] B. Wang, X.L. Lv, D. Feng, et al., J. Am. Chem. Soc. 138 (2016) 6204–6216.
[28] H. Malik, P.K. Iyer, ACS Appl. Mater. Interfaces 9 (2017) 4433–4439.
[29] K.E. Knowles, M. Malicki, E.A. Weiss, J. Am. Chem. Soc. 134 (2012) 12470–12473.
[30] W. Chi, J. Chen, W. Liu, et al., J. Am. Chem. Soc. 142 (2020) 6777–6785.